Atmos. Chem. Phys. Discuss., 14, 24087–24118, 2014
www.atmos-chem-phys-discuss.net/14/24087/2014/
doi:10.5194/acpd-14-24087-2014

Atmospheric Chemistry and Physics Discussions
Open Access

Sensitivity study of the aerosol effects on a supercell storm throughout its lifetime

A. Takeishi and T. Storelvmo

Department of Geology and Geophysics, Yale University, 210 Whitney Avenue, New Haven, CT 06511, USA

Received: 11 July 2014 – Accepted: 22 August 2014 – Published: 18 September 2014

Correspondence to: A. Takeishi (azusa.takeishi@yale.edu)

Published by Copernicus Publications on behalf of the European Geosciences Union.

Abstract

An increase in atmospheric aerosol loading could alter the microphysics, dynamics, and radiative characteristics of deep convective clouds. Earlier modeling studies have shown that the effects of increased aerosols on the amount of precipitation from deep convective clouds are model-dependent. This study aims to understand the effects of increased aerosol loading on a deep convective cloud throughout its lifetime with the use of the Weather Research and Forecasting (WRF) model as a cloud-resolving model (CRM). It simulates an idealized supercell thunderstorm with 8 different aerosol loadings, for three different cloud microphysics schemes. Variation in aerosol concentration is mimicked by varying either cloud droplet number concentration or the number of activated cloud condensation nuclei. We show that the sensitivity to aerosol loading is dependent on the choice of microphysics scheme. For the schemes that are sensitive to aerosols loading, the production of graupel via riming of snow is the key factor determining the precipitation response. The formulation of snow riming depends on the microphysics scheme and is usually a function of two competing effects, the size effect and the number effect. In many simulations, a decrease in riming is seen with increased aerosol loading, due to the decreased droplet size that lowers the riming efficiency drastically. This decrease in droplet size also results in a delay in the onset of precipitation, as well as so-called warm rain suppression. Although these characteristics of convective invigoration (Rosenfeld et al., 2008) are seen in the first few hours of the simulations, variation in the accumulated precipitation mainly stems from graupel production rather than convective invigoration. These results emphasize the importance of accurate representations of graupel formation in microphysics schemes.

1 Introduction

Interactions between aerosols and clouds remain one of the largest uncertainties in the projections of future climate (Myhre et al., 2013). Cloud droplets always form on

Discussion Paper | Discussion Paper | Discussion Paper | Discussion Paper |

ACPD

14, 24087–24118, 2014

Sensitivity study of the aerosol effects on a supercell storm

A. Takeishi and T. Storelvmo

aerosol particles, which lower the energy barrier for the phase transition from vapor to liquid by acting as cloud condensation nuclei (CCN). This implies that clouds forming in polluted air, such as urban air outflow and forest fire smoke, could differ from clouds forming in clean air in terms of droplet number concentration. The first indirect effect, or Twomey effect, refers to the decrease in cloud droplet size with increased aerosols and the resultant increase in cloud albedo (Twomey, 1977). Albrecht (1989) proposed that this decrease in droplet size lowers the collision and coalescence efficiency among cloud droplets, leading to a longer lifetime of clouds in polluted regions (the second indirect effect). Moreover, the effect of absorbing aerosols on clouds, or the semi-direct effect, has been a topic of growing interest in recent years (Hansen et al., 1997; Koren et al., 2004). These effects are all referred to as aerosol–cloud interactions (aci) in Boucher et al. (2013), while in the climate system both aci and aerosol–radiation interactions (ari) contribute to the radiation budget. Aerosol–cloud-precipitation interactions are quite complex, and Stevens and Feingold (2009) attribute this complexity to the buffering of clouds and the climate systems to aerosol perturbations; some forcings may act to oppose others and as a result the effects seem quite small in total. An accurate representation of the interactions is necessary for reducing the uncertainty in the future climate projections.

Although these microphysical effects of aerosols may alter properties of any cloud type, the interaction between aerosols and deep convective clouds are especially uncertain. Due to their short lifetime, small horizontal scale, and vigorous vertical motion, limited observations of deep convective clouds are available. However, deep convective clouds provide substantial amounts of precipitation in the tropics and midlatitudes over the summer continents, and modify the local and regional atmospheric circulations. Also, anvil clouds that originate from deep convection spread horizontally and cover a wide region around the convective core, altering the local radiation balance. These facts suggest a strong influence of aerosol microphysical effects on climate through deep convection, by alteration of precipitation, circulation, and radiation. Many recent studies have investigated the effects of aerosols on deep convective clouds, from ob-

ACPD
14, 24087–24118, 2014

servational, theoretical, and modeling points of view. Tao et al. (2012) recently summarized our current understanding of aerosol-deep convection interactions. They state that the majority of the observational studies suggest an increase in precipitation with aerosol loading, both from in situ measurement and satellite observations. Andreae et al. (2004), for example, observed a delay in the onset of precipitation, as well as strengthened updrafts in the area of Amazon under the influence of forest fire smoke. Niu and Li (2012) showed an increase in the precipitation rate and the cloud top height of mixed-phase clouds in the tropics with increased aerosols from satellite data.

Rosenfeld et al. (2008) presented the principle of convective invigoration using a conceptual model; smaller cloud droplets lead to a lower efficiency of collision and coalescence, resulting in warm rain suppression in the polluted air. Lifted cloud drops eventually freeze, increasing the amount of cold rain production, as well as the latent heat release aloft. This additional latent heat release strengthens the vertical motion of the storm and invigorates the entire storm system. This concept can explain the observed delay in precipitation initiation, as well as increased precipitation, with increased aerosol loading. In modeling studies, however, invigoration of convection does not always take place. Morrison (2012), hereinafter M12, examined the effects of aerosols on an idealized supercell with the Weather Research and Forecasting (WRF) model in a similar configuration to that in this study; the major differences lie in the vertical resolution (z coordinate in M12 and eta coordinate in our study) and the integration time (2 h in M12 and 10 h in our study). In M12, suppression of precipitation with increasing aerosol loading was seen. In another WRF study with configurations of the simulations nearly identical to that of M12 except for the wind profile, Nissan and Toumi (2013) showed an increase in precipitation when aerosol loading increases. Van den Heever and Cotton (2007) showed a strong dependence of aerosol–cloud interaction on the background aerosol concentration. They also found a strong impact of giant CCN on the development of warm rain that this study does not consider. Vertical wind shear is also considered to be an important factor. Fan et al. (2009) showed in their simulations that the vertical wind shear determines whether increased aerosol loading suppresses

ACPD
14, 24087–24118, 2014

or invigorates precipitation from deep convective clouds. Thus, modeling studies vary in the changes in precipitation with aerosol loading.

Most of the modeling studies so far had either fine spatial resolutions in short model runs, or relatively coarse resolutions for longer model runs, since long simulations with fine resolution are computationally expensive and require a lot of data storage. Horizontal and vertical resolutions ideally ought to be high enough to resolve convective clouds, so that convective parameterization schemes are not necessary. At the same time, Tao et al. (2012) states that *"These results suggest that model simulations of the whole life cycle of a convective system are needed in order to assess the impact of aerosols on precipitation processes associated with mesoscale convective systems (MCSs) and thunderstorms"*. In order to satisfy both of these requirements, long simulations with fine resolutions are necessary. Also, the model domain has to be large enough to include the spreading anvil clouds and cold pool. In addition to these requirements for resolution and run time, variations of aerosol concentration in simulations should cover the wide range of realistic aerosol loadings in the atmosphere. In most studies to date, however, the variation is represented by only a few aerosol concentrations. Simulations with more than a couple of different concentrations would enable us to understand the aerosol effects in greater detail. Furthermore, it is of interest to know how results vary depending on the choice of the microphysics scheme. If simulations meet these requirements, the results would have the potential to resolve the discrepancy between observations and models, as well as among models, and indicate possible improvements for modeling studies.

This study aims to understand the effects of increased aerosols on deep convection while taking the above points into consideration. With fine horizontal resolutions, we simulate a deep convective cloud in a large domain for 10 h within which precipitation terminates in most of the cases. Although our simulations do not include explicit aerosol activation, our simulations represent 8 different aerosol loadings with three different microphysics schemes. To confirm the robustness of the results, we examine the results in several different model configurations.

ACPD
14, 24087–24118, 2014

A. Takeishi and T. Storelvmo

2 Methods

2.1 Simulation setup

This study uses the WRF model version 3.2.1 (Skamarock et al., 2008). Our simulations are based on the quarter-circular shear supercell case that is publicly available for download (http://www2.mmm.ucar.edu/wrf/users/downloads.html). In order to simulate the storm throughout its whole lifetime, the domain is enlarged and simulations run for 10 h with periodic boundary conditions. The size of the domain is 600 km × 600 km with a rigid lid at 20 km high. The uppermost 5 km experiences Rayleigh damping with a damping coefficient of 0.003 s^{-1}. The horizontal resolution is 1 km and there are 40 vertical levels. The time step is 6 s. As the eta coordinate is employed, the highest vertical resolution is approximately 210 m in the lowest atmosphere. With this fine resolution, convective clouds are resolved and the model is treated as a cloud-resolving model (CRM). The base atmospheric sounding used to initialize the model is shown in Fig. 1a. The wind and temperature profiles are the same as those of Weisman and Klemp (1982). However, the moisture profile is modified so that the environment is dry enough for the storm activity to terminate, or precipitation rates to decrease, within 10 h. This base profile has a convective available potential energy (CAPE) of approximately 600 J kg^{-1}. In order to trigger convection, the initial temperature profile is modified in the center of the domain (Fig. 1c). This "heating" has a horizontal radius of 10 km and extends up to approximately 1.5 km high with the perturbation maximum of 2 K at the lowest level of the atmosphere. To provide a moisture source for precipitation and produce a gradual transition in CAPE toward the center, the moisture profile is modified relative to that of Weisman and Klemp (1982) in the center of the domain with the radius of 15 km (Fig. 1b). As a result, the "heated" area has a CAPE of approximately 2500 J kg^{-1} and the "moisture ring" that surrounds the heated area has a CAPE of approximately 2000 J kg^{-1} (Fig. 1d). In addition, relatively strong friction is imposed on the lowest level of the atmosphere with a friction coefficient C_D of 0.01. According to Table 9.2 in Wallace and Hobbs (2006), a drag coefficient of 0.012 represents a rough

ACPD
14, 24087–24118, 2014

land surface. Radiation, the Coriolis force, and the land surface schemes are turned off. It is emphasized that the goal of this study is to understand the effects of aerosols on deep convection throughout the lifetime of a storm. For this reason, the domain is much larger than the characteristic scale of a supercell, the base sounding is relatively dry, and relatively strong drag is added.

2.2 Microphysics schemes and sensitivity tests

An increase in aerosol concentration generally results in an increase in CCN and cloud droplets. Because none of the microphysics schemes in WRF 3.2.1 include an aerosol activation scheme, we examine the effect of increasing aerosols by increasing either the number of activated CCN or the cloud droplet number concentration, depending on the microphysics scheme employed. Three microphysics schemes, the Morrison (Morrison et al., 2009), the Milbrandt–Yau (Milbrandt and Yau, 2005), and the Thompson (Thompson et al., 2008) schemes, are chosen for this study.

The Morrison scheme includes water vapor and five types of hydrometeors as prognostic variables; liquid cloud drops, rain, ice crystals, snow, and either graupel or hail. Hail is chosen for this study as is recommended for continental deep convection studies. The Milbrandt–Yau scheme includes water vapor and six types of hydrometeors; liquid cloud drops, rain, ice crystals, snow, graupel, and hail. The Thompson scheme includes water vapor and five types of hydrometeors; liquid cloud drops, rain, ice crystals, snow, and graupel. All of these microphysics schemes are two-moment schemes; in other words, they calculate both mass mixing ratios and number concentrations of hydrometeors.

In the Morrison scheme and the Thompson scheme, cloud droplet number concentration is prescribed. The concentration of $250\,\mathrm{cm^{-3}}$ is set as a control. In this study this concentration is multiplied by 0.2, 0.5, 2, 3, 4, 5, or 6, so that 2 clean cases and 5 polluted cases are simulated in addition to the control case.

In the Milbrandt–Yau scheme, the concentration of activated CCN is calculated, based on its relationship with supersaturation. This relationship is obtained from sim-

ACPD
14, 24087–24118, 2014

A. Takeishi and T. Storelvmo

ulations of aerosol activation (Cohard et al., 1998). In order to mimic the increase or decrease in aerosols, the equation that calculates the number of activated CCN is multiplied by 0.2, 0.5, 2, 3, 4, 5, or 6.

Thus, simulations with different microphysics schemes mimic the changes in aerosol concentration differently. As a result, the simulation results are not directly comparable. However, given the initial changes that we make, the results are still qualitatively comparable. Hereinafter, a change in the number of activated CCN or cloud droplet number concentration is taken as equivalent to a change in the number of aerosols.

2.3 Robustness evaluation

In order to check the robustness of the simulation results, the maximum heating of 2 K in the standard setup is modified to 1 K or 3 K in additional simulations, representing a weaker or stronger heat perturbation, respectively. Also, runs with 2 km horizontal resolution are carried out. In addition, simulations with no initial horizontal winds were included so that the effects of winds and strong vertical wind shear are assessed. For the Morrison scheme, additional simulations with graupel, instead of hail, are also carried out. Moreover, test simulations without melting of certain hydrometeors were done, to help us understand how much precipitation comes from hail, graupel, or snow. We acknowledge that these simulations are unphysical, and they were performed exclusively to aid the interpretation of the other simulations.

Thus, we have simulated a supercell storm with 21 different configurations with 8 different concentrations of aerosols in each case, for a total of 168 simulations (Table 1).

3 Results and discussions

3.1 Morrison scheme

Figure 2a shows the time evolution of domain-average accumulated precipitation in different runs with the Morrison scheme. According to this figure, precipitation termi-

ACPD
14, 24087–24118, 2014

nates within 5 h in all of the runs. This is confirmed by the maximum and minimum vertical velocities in Fig. 2b. The total precipitation amount decreases with the increase in aerosol concentration, although not in a completely systematic way, which is also indicated by the vertical velocities to some extent. This tendency agrees with the results in M12, though the simulations run longer in this study. This decrease is, however, not a robust response (Fig. 2c–h); we see no pattern in the amount of precipitation that is common among runs with different configurations. Also, the differences in the amount of precipitation among runs are quite small in the first few hours. This fact emphasizes the importance of simulating the entire life cycle of deep convection for understanding the full effects of aerosols. The lifetime of the storm, differences in precipitation, and the amount of precipitation are all much smaller in the no-wind simulations. This is expected, because without shear the precipitation in the storm easily reduces the updraft and yields a shorter lifetime than when vertical wind shear is included. Due to the lack of systematic changes in accumulated precipitation with aerosol loading, it is fair to say that this scheme does not have a high sensitivity to aerosol loading, or alternatively aerosol effects are compensated for by other factors as is mentioned by M12.

3.2 Milbrandt–Yau scheme

3.2.1 change in accumulated precipitation

The Milbrandt–Yau scheme differs from the other two schemes in that it does not prescribe the cloud droplet number concentration. Instead, it employs a relationship between the number of activated CCN and supersaturation, which is derived by Cohard et al. (1998). Variation in cloud droplet number concentration makes the simulations more realistic. Moreover, this scheme includes both graupel and hail as prognostic variables. Because the density and terminal fall velocity of the two hydrometeors are quite different, this also makes the scheme more realistic. Figure 3a and b shows the time evolution of accumulated precipitation and vertical velocities in all 8 cases, respectively. It is readily seen that the cleanest case gives by far the largest amount

ACPD
14, 24087–24118, 2014

of precipitation. The other runs do not seem to show a simple systematic ordering in this figure. However, all of the runs show some robust feature in the accumulated precipitation with increased aerosol loading (Fig. 3c–g); precipitation is the largest in the cleanest case, and it decreases as aerosol increases, and then slightly increases again at intermediate aerosol concentration. This "U-shape" pattern in the change in accumulated precipitation is seen in all of the simulations, regardless of heating, horizontal resolution, or winds, though the aerosol concentration with minimum precipitation depends on the simulation configuration. Note that two additional simulations, 2.5 and 3.5 times control, are done for the standard case, in order to confirm the robustness of this U-shape pattern. The maximum and minimum vertical velocities seem to be tightly connected to the amount of precipitation. This is expected, because evaporation of rain creates a stronger downdraft and cold pool that can invigorate the convection.

The amount of frozen precipitation changes with aerosol loading as well. Figure 4 shows the time evolution of horizontally averaged hail mixing ratio. It is clear that the amount of hail that reaches the surface increases with aerosol loading.

3.2.2 Physical interpretation

To understand how the change in aerosol affects the amount of precipitation in this scheme, we firstly examined which hydrometeor most of the surface precipitation originates from. This cannot be readily seen because frozen precipitation, such as snow, graupel, and hail, melts by the time it reaches the surface. Some additional simulations are done in which certain frozen hydrometeors do not melt; hail, hail and graupel, or hail, graupel, and snow. Note that in the runs without graupel melting, for example, hail does not melt so that once graupel forms the mass stays frozen until it reaches the surface, even after it is transformed to hail. In this way we estimate the contribution of each frozen hydrometeor to surface precipitation. It should be noted, however, that the results cannot be analyzed completely quantitatively. Only if the majority of surface precipitation turns into frozen precipitation (or stays liquid) in these tests can we conclude that the hydrometeor is (not) responsible for most of precipitation. This is because the

ACPD
14, 24087–24118, 2014

lack of latent heat used for melting and increased terminal fall velocity could change the dynamics of the storm.

The runs without melting of hail are quite similar to the standard runs in terms of frozen precipitation at the surface (not shown). However, the runs without melting of graupel and hail have more than 90 % of the precipitation reaching the surface as frozen (Fig. 5). In other words, liquid precipitation drastically decreased once both graupel and hail were prevented from melting. With this drastic change in the type of surface precipitation in these runs, it is clear that most of the precipitation starts as graupel. This is also confirmed by comparing the time evolution of horizontally averaged graupel mixing ratio with that of rain mixing ratio (Fig. 6). The question arises as to why the amount of graupel changes with aerosol loading. Graupel forms by the riming of snow in this scheme, and the riming rate is a function of four key variables that change with aerosol concentrations; riming efficiency, number of snow crystals, number of cloud droplets, and the size of cloud drops. The following equation, Eq. (19) in Milbrandt and Yau (2005), calculates the riming rate $\mathrm{QCL_{cs}}$ in the Milbrandt–Yau scheme;

$$\mathrm{QCL_{cs}} = \frac{k_0}{\rho^a} E_{\mathrm{sc}} N_{\mathrm{Ts}} N_{\mathrm{Tc}} \times \left[\frac{k_1}{\lambda_{\mathrm{s}}{}^{k_2} \lambda_{\mathrm{c}}{}^{k_3}} + \frac{k_4}{\lambda_{\mathrm{s}}{}^{k_5} \lambda_{\mathrm{c}}{}^{k_6}} + \frac{k_7}{\lambda_{\mathrm{s}}{}^{k_8} \lambda_{\mathrm{c}}{}^{k_9}} \right] \quad (1)$$

where a and k_n ($n = 0\ldots9$) are constants, ρ is air density, E_{sc} is the riming efficiency, N_{Ts} and N_{Tc} are the total number concentrations of snow crystals and cloud droplets, respectively, and λ_{s} and λ_{c} are the slope parameters for the snow and droplet size distributions, respectively. The riming efficiency is calculated based on Figs. 14–11 in Pruppacher and Klett (1997), and slope parameters decrease as the corresponding hydrometeor size increases. Thus, E_{sc} and the terms in the square bracket become smaller as aerosol increases, whereas the two number concentration terms become larger. Hereinafter the former is called the size effect and the latter is called the number effect. The change in the amount of graupel is determined as a result of these two competing effects; as aerosols increase, each cloud droplet becomes smaller, and the riming efficiency and the growth rate decrease. At the same time, however, the chances

ACPD
14, 24087–24118, 2014

of riming increase because the number of cloud droplets and snow crystals increase. This competition results in the U-shape pattern in the precipitation. The cleaner cases have a strong size effect, whereas the polluted cases have a strong number effect. In the intermediate aerosol concentration case in which the least amount of the precipitation is found, the size is not large enough for a strong size effect and the number of cloud drops is not large enough for a strong number effect. This result shows the importance of snow riming in understanding aerosol-deep convection interactions in this scheme, and is consistent with Tao et al. (2012). Some of the runs do not perfectly follow this U-shape pattern. This is likely due to the fact that towards the end of the simulations droplet concentration does not necessarily decrease completely systematically with increased aerosol loadings; in some runs (the 4*control, 5*control, and 6*control runs in the standard simulations, the 5*control run in the 1 K simulations, and the 6*control run in the 2 km simulations) a drastic decrease in the *domain-averaged* droplet concentration is seen later in the simulations (around 5, 5, and 7 h after the beginning, respectively, in Fig. 7). These anomalously low droplet concentrations could be the reason for the deviations from the U-shape in these runs. Indeed, the U-shape pattern becomes even clearer if we do not take these runs into account. Relatively short lifetimes and anomalously lower *in-cloud* droplet concentration both seem to be the reason for this drastic decrease in the *domain-average* droplet concentration. Cold pool strength, defined as the lowest temperature at 200 m height in this study, strengthens as precipitation increases (not shown). This is due to the increased melting and evaporation of precipitation. As the cold pool propagates, new convection is induced at the cold pool front, but in our study this is dry convection due to the relatively dry sounding.

Even though the above argument shows that graupel is the key hydrometeor for precipitation formation in the simulations, the change in the amount of hail reaching the surface is also an important factor to consider, because of the severe damage hail could have on infrastructure on the ground. The increase in the amount of hail with aerosol loading is attributable to the increase in lifted cloud drops (Fig. 8); because of the

ACPD
14, 24087–24118, 2014

reduced size of cloud drops, the collision-coalescence efficiency decreases, leading to a decrease in warm rain production and more cloud drops available for riming aloft. This is consistent with Rosenfeld et al. (2008). This warm rain suppression, as well as the delay in the onset of precipitation, is seen in Figs. 3a and 5. As a result, more hail forms aloft by riming and reaches the surface in the polluted cases. However, this effect is seen only in the first two hours of the simulations. This may be because after a few hours vertical velocity is no longer high enough (Fig. 3b) to transport sufficient cloud droplets upward for formation of hail through riming (Fig. 8). Since only large graupel can become hail, large amount of droplets aloft is necessary for hail formation. After a few hours, cold precipitation through the graupel production becomes a dominant factor controlling the amount of precipitation, as explained above.

3.3 Thompson scheme

3.3.1 Change in accumulated precipitation

Figure 9a shows the time evolution of accumulated precipitation in the runs with the Thompsons scheme. All of the runs stop precipitating within 10 h, and there seems to be a decrease in precipitation with increased aerosols, though the vertical velocities hardly show this tendency (Fig. 9b). This pattern turns out to be robust only in the first 4 h (Fig. 9c–g). Although this study aims to understand the aerosol effect throughout the lifetime of deep convection, it is also meaningful to understand this tendency in the first 4 h as this is when the highest precipitation rates occur, and hence when the risk of flooding and rapid soil erosion is possible.

3.3.2 Physical interpretation

As we did for the runs with the Milbrandt–Yau scheme, additional simulations without melting of certain hydrometeors are done (Table 1); without melting graupel, or without melting snow and graupel. Runs without melting graupel gives quite high percentages

ACPD
14, 24087–24118, 2014

of frozen precipitation in the first half of the simulations (Fig. 10). This indicates that the runs with the Thompson scheme also get most of the precipitation from graupel, as is confirmed by Fig. 11. Also, in the Thompson scheme riming of snow is the principal graupel production mechanism, and the riming rate is a function of riming efficiency, snow crystal size, snow number concentration, and mixing ratio of cloud droplets. This is different from the formulation in the Milbrandt–Yau scheme in that it uses mass of liquid in the cloud as a variable, instead of the number of cloud droplets. Although liquid water content increases with aerosols due to the reduced efficiency in collision-coalescence and warm rain production, its change with aerosol loading is much smaller than that of cloud droplet number concentration. As a result, the size effect is dominant in the runs with the Thompson scheme, resulting in the decrease in accumulated precipitation in the first 4 h.

4 Conclusions

The effects of increased aerosols on deep convective clouds, as well as its dependence on the microphysics scheme, are examined with the use of WRF. By varying either cloud droplet concentration or the number of activated CCN, 8 simulations with different "aerosol concentration" are carried out for each microphysics scheme. One of the most important aims of this study was to simulate a storm throughout its lifetime including the termination of precipitation.

It is clear that depending on the microphysics scheme, the response to aerosol perturbation greatly differs. The Morrison scheme seems to be either insensitive to aerosol perturbations or other effects compensate for any loss or excess of precipitation. The Milbrandt–Yau scheme showed a strong dependence on the aerosol concentration. We showed that the precipitation mainly starts as graupel, and the graupel production is a result of a delicate balance between the size effect and the number effect. Simulations with the Thompson scheme showed the dominance of the size effect in the first 4 h, but after ten hours the change in precipitation is not systematic. Thus, the aerosol-

ACPD
14, 24087–24118, 2014

deep convection interaction in a model, as well as the absolute amount of precipitation, is strongly dependent on the microphysics scheme. Figure 12 shows the storm evolution in the cleanest case after 2, 4, 6, and 10 h of simulations with each of the three microphysics schemes. The behavior and the lifetime of the clouds are clearly different, depending on the microphysics scheme.

As Cheng et al. (2010) show in their Fig. 11, there are mainly four microphysical ways in which an aerosol increase can affect precipitation; so-called warm rain suppression (Effect-A), reduction in riming efficiency (Effect-B), more liquid water aloft (Effect-C), and more freezing aloft (Effect-D). Especially in our runs with the Milbrandt–Yau and Thompson schemes, we showed that the Effect-A and Effect-B dominated over the Effect-C and Effect-D, though the number effect also plays a role in the Milbrandt–Yau scheme. This dominance of certain effects is again dependent on the microphysics schemes.

Note that some mechanisms are not entirely clear, due to the complexity of cloud microphysics. Precipitation in the latter 6 h of the Thompson runs changes unsystematically with aerosol loading, as opposed to the systematic change in the first 4 h. Also, the runs with the Milbrandt–Yau scheme vary in what aerosol concentration produces the minimum in the U-shape pattern, depending on the simulation configurations. It should be noted that this study did not explicitly separate the microphysical and dynamical effects that are both caused by the differences in aerosol loading, as they are tightly connected to each other. For instance, an increase in graupel production contributes to an increase in precipitation, cold pool strength, and updraft and downdraft velocities, which enhances precipitation even more. Also, it is not conclusive from our analysis which could change the surface precipitation more drastically; differences in heating or differences in aerosol concentrations. In our study the presence of the vertical wind shear did not change the microphysical response, though the lifetime was much shorter for the no-shear cases. This does not agree with Fan et al. (2009), but more gradual change in shear, as well as detailed analysis, is needed to assess the actual role of shear in this study. In our simulations the cold pool does not trigger new moist con-

ACPD
14, 24087–24118, 2014

vection, as the environmental sounding is relatively dry so that the cloud system stops precipitating. However, this is not always the case in reality, as the cold pool propagation may sometimes feed new convective clouds. Entrainment is another process that is important in cloud development, as well as in determining aerosol concentration, which our study did not focus on. Fridlind et al. (2004) showed that mid-tropospheric aerosols are the primary nuclei of anvil crystals, indicating the importance of entrainment and detrainment.

This modeling study has presented the aerosol effects on deep convection with three different WRF microphysics schemes, and we offer physical interpretations of the results. In contrast to our modeling results, however, invigoration of convection is often observed. If we attribute it to the convective invigoration proposed by Rosenfeld et al. (2008), then the graupel formation possibly has an excessive influence on precipitation in WRF, especially in the Milbrandt–Yau and the Thompson schemes, though the warm rain suppression is well reproduced. This excessive graupel influence could possibly be avoided by having gradual and weaker heating of the surface air, instead of having a strong heat bubble, since weaker upward motion would allow more production of warm rain and therefore less cold rain production mainly coming from graupel. Thus, tendencies and characteristics of simulation configurations, as well as cloud microphysics schemes, can have a strong impact on the simulated aerosol effect of deep convection. These dependencies should be kept in mind in future modeling studies. Ultimately, the discrepancies between different microphysics schemes, as well as between modeled and observed aerosol effects on deep convection, should be resolved. This could be achieved with field observations of deep convective clouds and subsequent numerical modeling of selected cases, using different microphysics schemes. However, such cases will only be helpful in constraining models and parameterization schemes if they are well characterized both in terms of aerosol and cloud properties.

ACPD
14, 24087–24118, 2014

References

Albrecht, B. A.: Aerosols, cloud microphysics, and fractional cloudiness, Science, 245, 1227–1230, 1989.
Andreae, M. O., Rosenfeld, D., Artaxo, P., Costa, A. A., Frank, G. P., Longo, K. M., and Silva-Dias, M. A. F.: Smoking rain clouds over the Amazon, Science, 303, 1337–1342, 2004.
Boucher, O., Randall, D., Artaxo, P., Bretherton, C., Feingold, G., Forster, P., Kerminen, V.-M., Kondo, Y., Liao, H., Lohmann, U., Rasch, P., Satheesh, S. K., Sherwood, S., Stevens, B., and Zhang, X. Y.: Clouds and aerosols, in: Climate Change 2013: The Physical Science Basis. Contribution of Working Group I to the Fifth Assessment Report of the Intergovernmental Panel on Climate Change, edited by: Stocker, T. F., Qin, D., Plattner, G.-K., Tignor, M., Allen, S. K., Boschung, J., Nauels, A., Xia, Y., Bex, V., and Midgley, P. M., Cambridge University Press, Cambridge, UK and New York, NY, USA, 2013.
Cheng, C.-T., Wang, W.-C., and Chen, J.-P.: Simulation of the effects of increasing cloud condensation nuclei on mixed-phase clouds and precipitation of a front system, Atmos. Res., 96, 461–476, 2010.
Cohard, J.-M., Pinty, J.-P., and Bedos, C.: Extending Twomey's analytical estimate of nucleated cloud droplet concentrations from CCN spectra, J. Atmos. Sci., 55, 3348–3357, 1998.
Fan, J., Yuan, T., Comstock, J. M., Ghan, S., Khain, A., Leung, L. R., Li, Z., Martins, V. J., and Ovchinnikov, M.: Dominant role by vertical wind shear in regulating aerosol effects on deep convective clouds, J. Geophys. Res., 114, D22206, doi:10.1029/2009JD012352, 2009.
Fridlind, A. M., Ackerman, A. S., Jensen, E. J., Heymsfield, A. J., Poellot, M. R., Stevens, D. E., Wang, D., Miloshevich, L. M., Baumgardner, D., Lawson, R. P., Wilson, J. C., Flagan, R. C., Seinfeld, J. H., Jonsson, H. H., VanReken, T. M., Varutbangkul, V., and Rissman, T. A.: Evidence for the predominance of mid-tropospheric aerosols as subtropical anvil cloud nuclei, Science, 304, 718–722, 2004.
Hansen, J., Sato, M., and Ruedy, R.: Radiative forcing and climate response, J. Geophys. Res., 102, 6831–6864, 1997.
Koren, I., Kaufman, Y. J., Remer, L. A., and Martins, J. V.: Measurement of the effect of Amazon smoke on inhibition of cloud formation, Science, 303, 1342–1345, 2004.
Milbrandt, J. A., and Yau, M. K.: A multimoment bulk microphysics parameterization. Part II: A proposed three-moment closure and scheme description, J. Atmos. Sci., 62, 3065–3081, 2005.

Morrison, H.: On the robustness of aerosol effects on an idealized supercell storm simulated with a cloud system-resolving model, Atmos. Chem. Phys., 12, 7689–7705, doi:10.5194/acp-12-7689-2012, 2012.

Morrison, H., Thompson, G., and Tatarskii, V.: Impact of cloud microphysics on the development of trailing stratiform precipitation in a simulated squall line: comparison of one- and two-moment schemes, Mon. Weather Rev., 137, 991–1007, 2009.

Myhre, G., Shindell, D., Bréon, F.-M., Collins, W., Fuglestvedt, J., Huang, J., Koch, D., Lamarque, J.-F., Lee, D., Mendoza, B., Nakajima, T., Robock, A., Stephens, G., Takemura, T., and Zhang, H.: Anthropogenic and Natural Radiative Forcing, in: Climate Change 2013: The Physical Science Basis. Contribution of Working Group I to the Fifth Assessment Report of the Intergovernmental Panel on Climate Change, edited by: Stocker, T. F., Qin, D., Plattner, G.-K., Tignor, M., Allen, S. K., Boschung, J., Nauels, A., Xia, Y., Bex, V., and Midgley, P. M., Cambridge University Press, Cambridge, UK and New York, NY, USA, 2013.

Nissan, H. and Toumi, R.: On the impact of aerosols on soil erosion, Geophys. Res. Lett., 40, 5994–5998, 2013.

Niu, F. and Li, Z.: Systematic variations of cloud top temperature and precipitation rate with aerosols over the global tropics, Atmos. Chem. Phys., 12, 8491–8498, doi:10.5194/acp-12-8491-2012, 2012.

Pruppacher, H. R. and Klett, J. D.: Microphysics of Clouds and Precipitation, Kluwer Academic Press, 1997.

Rosenfeld, D., Lohmann, U., Raga, G. B., O'Dowd, C. D., Kulmala, M., Fuzzi, S., Reissell, A., and Andreae, M. O.: Flood or drought: How do aerosols affect precipitation?, Science, 321, 1309–1313, 2008.

Skamarock, W. C., Klemp, J. B., Dudhia, J., Gill, D. O., Barker, D. M., Duda, M. G., Huang, X.-Y., Wang, W., and Powers, J. G.: A description of the advanced research WRF version 3, NCAR Tech. Note TN-475+STR, 113 pp., 2008.

Stevens, B. and Feingold, G.: Untangling aerosol effects on clouds and precipitation in a buffered system, Nature, 461, 607–613, 2009.

Tao, W.-K., Chen, J.-P., Li, Z., Wang, C., and Zhang, C.: Impact of aerosols on convective clouds and precipitation, Rev. Geophys., 50, RG2001, doi:10.1029/2011RG000369, 2012.

Thompson, G., Field, P. R., Rasmussen, R. M., and Hall, W. D.: Explicit forecasts of winter precipitation using an improved bulk microphysics scheme. Part II: Implementation of a new snow parameterization, Mon. Weather Rev., 136, 5095–5115, 2008.

ACPD
14, 24087–24118, 2014

Sensitivity study of the aerosol effects on a supercell storm

A. Takeishi and T. Storelvmo

Twomey, S.: The influence of pollution on the shortwave albedo of clouds, J. Atmos. Sci., 34, 1149–1152, 1977.
van den Heever, S. C. and Cotton, W. R.: Urban aerosol impacts on downwind convective storms, J. Appl. Meteorol. Clim., 46, 828–850, 2007.
Wallace, J. M. and Hobbs, P. V.: Atmospheric Science: An Introductory Survey, Academic Press, 2006.
Weisman, M. L. and Klemp, J. B.: The dependence of numerically simulated convective storms on vertical wind shear and buoyancy, Mon. Weather Rev., 110, 504–520, 1982.

ACPD
14, 24087–24118, 2014

Table 1. Simulations run in this study. Each case was simulated with 8 different aerosol concentrations.

Microphysics scheme	Description
Morrison	Standard
	Maximum heating of 1 K
	Maximum heating of 3 K
	Horizontal resolution of 2 km
	No initial wind
	Graupel instead of hail
Milbrandt–Yau	Standard
	Maximum heating of 1 K
	Maximum heating of 3 K
	Horizontal resolution of 2 km
	No initial wind
	No melting of hail
	No melting of graupel and hail
	No melting of snow, graupel, and hail
Thompson	Standard
	Maximum heating of 1 K
	Maximum heating of 3 K
	Horizontal resolution of 2 km
	No initial wind
	No melting of graupel
	No melting of snow and graupel

ACPD
14, 24087–24118, 2014

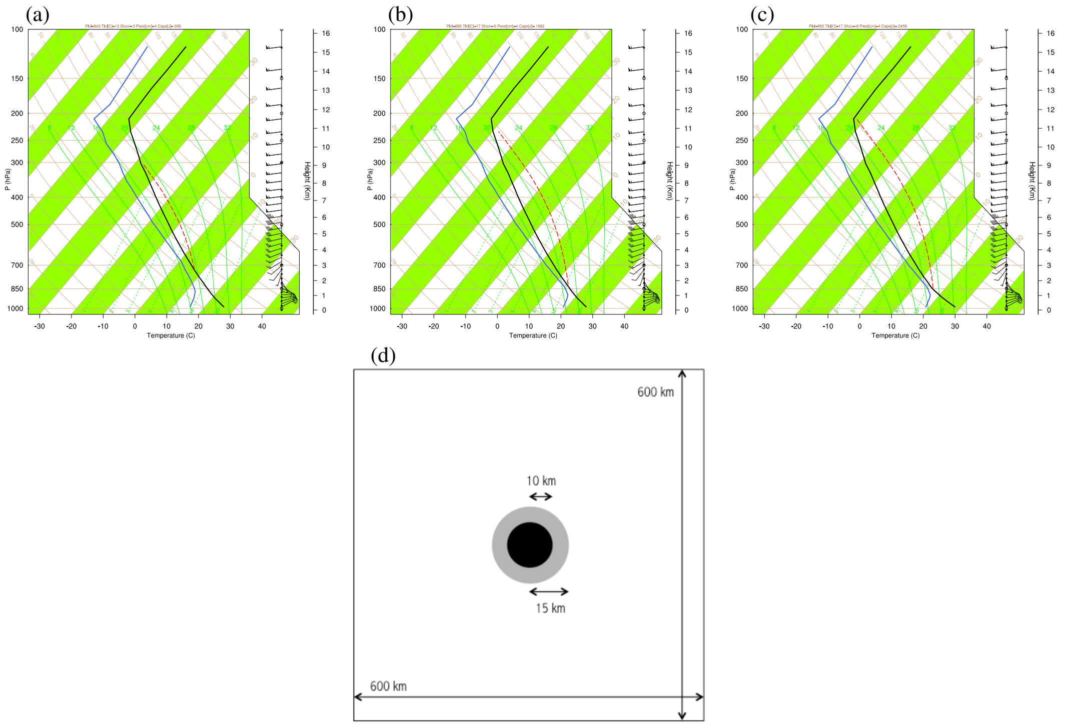

Figure 1. Skew-T log-P diagrams of **(a)** the base sounding, **(b)** the moisture ring, and **(c)** the heat bubble. The horizontal distribution of the different soundings in the domain is shown in **(d)**; the white area has the base sounding, the grey area has the moist sounding, and the black area has the heat bubble sounding. Note that the sizes of the domain, the moisture ring, and the heat bubble do not scale to each other in **(d)**.

ACPD
14, 24087–24118, 2014

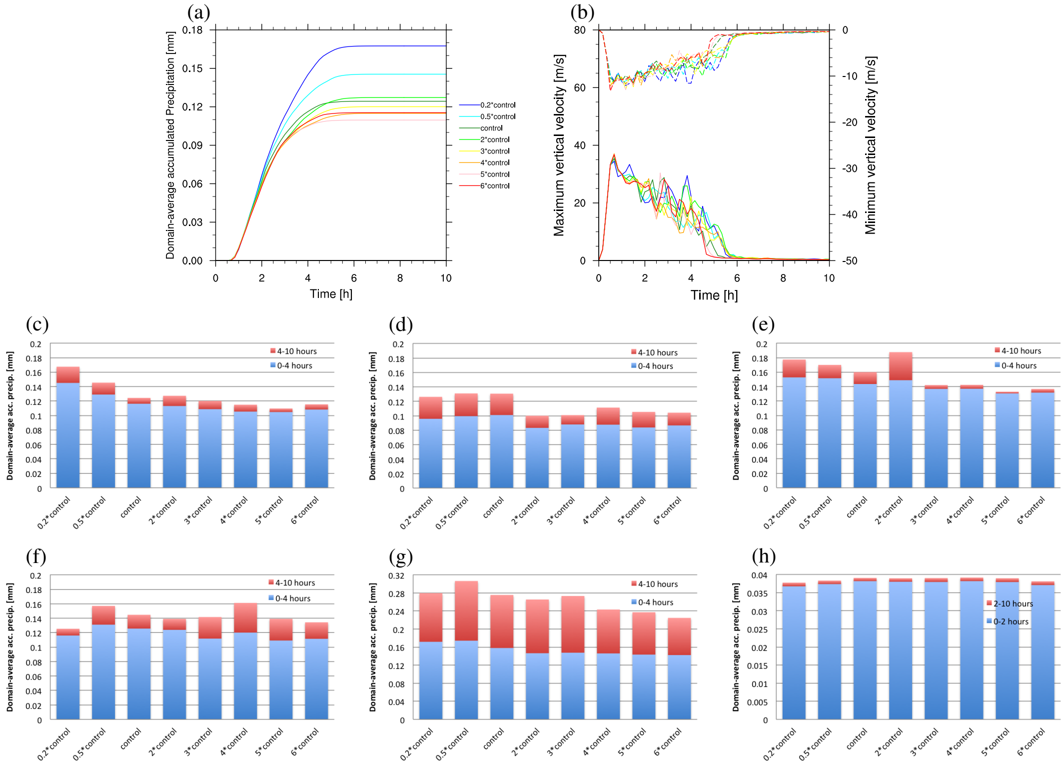

Figure 2. Results from simulations with the Morrison scheme; **(a)** time evolution of domain-average accumulated precipitation [mm] and **(b)** maximum (solid, left axis) and minimum (dashed, right axis) vertical velocities [$\mathrm{m\,s^{-1}}$]. Different colors show runs with different aerosol concentrations. In addition, domain-averaged accumulated precipitation in [mm] with different aerosol concentrations in the **(c)** standard, **(d)** 1 K-heating, **(e)** 3 K-heating, **(f)** 2 km-resolution, **(g)** graupel, and **(h)** no initial wind runs is shown.

ACPD
14, 24087–24118, 2014

Sensitivity study of the aerosol effects on a supercell storm

A. Takeishi and T. Storelvmo

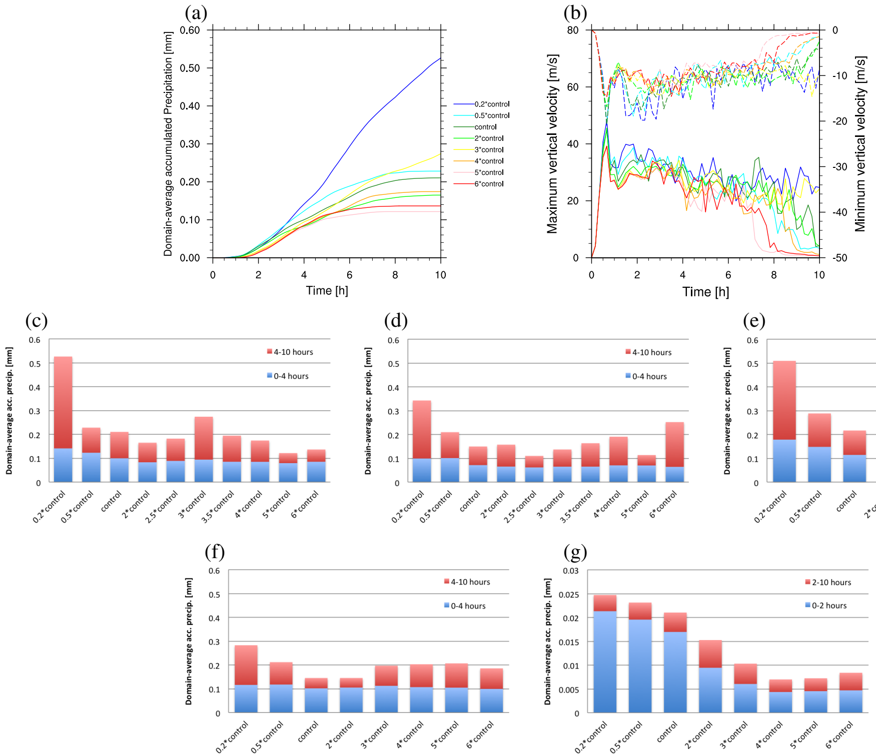

Figure 3. Results from simulations with the Milbrandt–Yau scheme; **(a)** time evolution of domain-average accumulated precipitation [mm] and **(b)** maximum (solid, left axis) and minimum (dashed, right axis) vertical velocities [$\mathrm{m\,s^{-1}}$]. Different colors show runs with different aerosol concentrations. In addition, domain-averaged accumulated precipitation in [mm] with different aerosol concentrations in the **(c)** standard, **(d)** 1 K-heating, **(e)** 3 K-heating, **(f)** 2 km-resolution, and **(g)** no initial wind runs is shown.

ACPD
14, 24087–24118, 2014

Sensitivity study of the aerosol effects on a supercell storm

A. Takeishi and T. Storelvmo

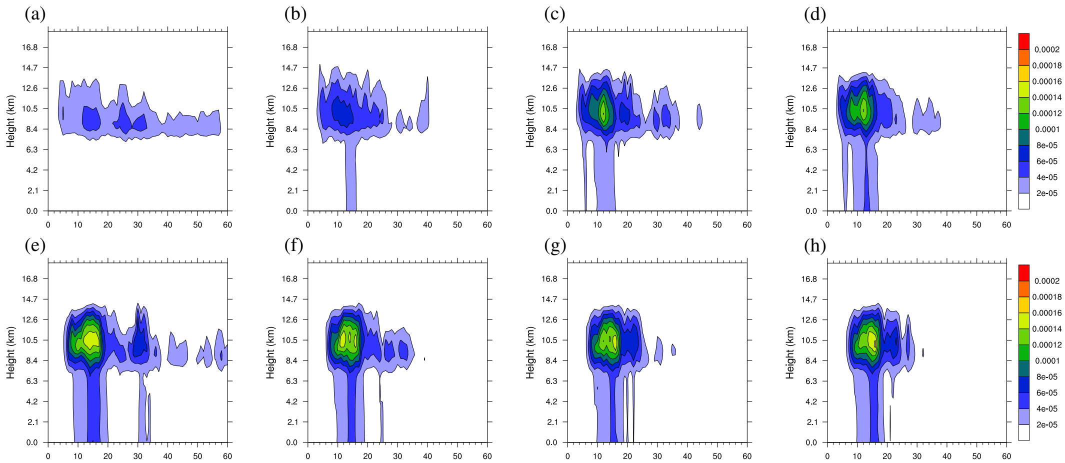

Figure 4. Time evolution of horizontally averaged hail mixing ratio [$\mathrm{g\,kg^{-1}}$] in 8 runs with different aerosol concentrations; **(a)** 0.2*control, **(b)** 0.5*control, **(c)** control, **(d)** 2*control, **(e)** 3*control, **(f)** 4*control, **(g)** 5*control, and **(h)** 6*control in the Milbrandt–Yau runs. The vertical axis is height in [km], while the horizontal axis is time in [10 min], thus 60 corresponds to 600 min = 10 h.

ACPD

14, 24087–24118, 2014

Title Page
Abstract | Introduction
Conclusions | References
Tables | Figures
◀| |▶
◀ ▶
Back | Close
Full Screen / Esc
Printer-friendly Version
Interactive Discussion

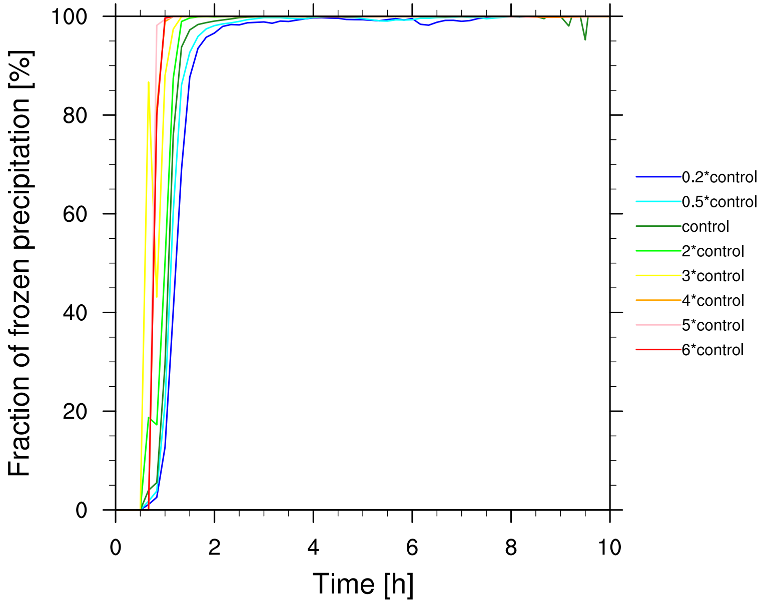

Figure 5. Time evolution of percentages [%] of frozen precipitation in total precipitation reaching the surface in the past 10 min, when graupel and hail do not melt in the runs with the Milbrandt–Yau scheme. If there is no surface precipitation in the past 10 min, the percentages are set to be zero. High percentages of frozen precipitation are seen, and the contribution of warm rain is implicitly indicated by the delayed rise in the fraction of frozen precipitation in cleaner cases.

ACPD
14, 24087–24118, 2014

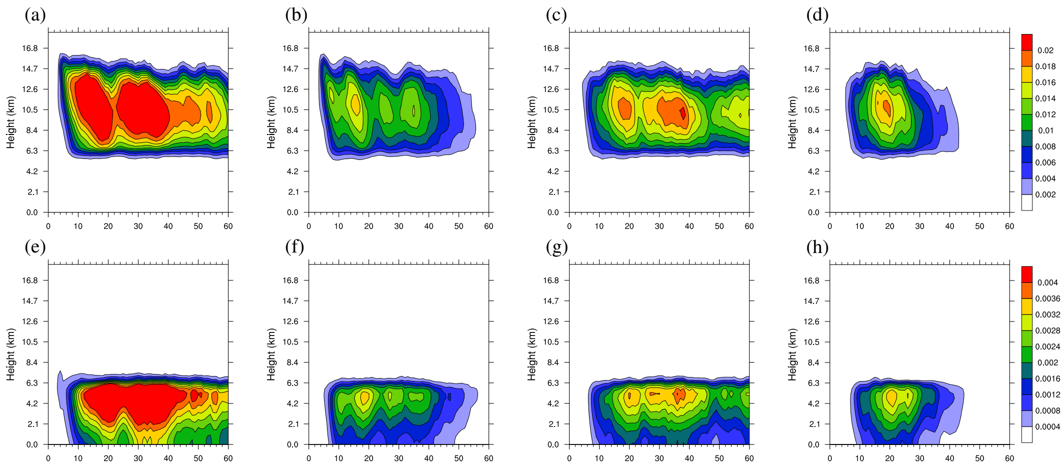

Figure 6. Time evolution of horizontally averaged graupel **(a–d)** and rain **(e–h)** mixing ratios [g kg^{-1}] in **(a, e)** 0.2*control, **(b, f)** control, **(c, g)** 3*control, and **(d, h)** 6*control runs with the Milbrandt–Yau scheme. The vertical axis is height in [km], while the horizontal axis is time in [10 min], thus 60 corresponds to 600 min = 10 h.

ACPD
14, 24087–24118, 2014

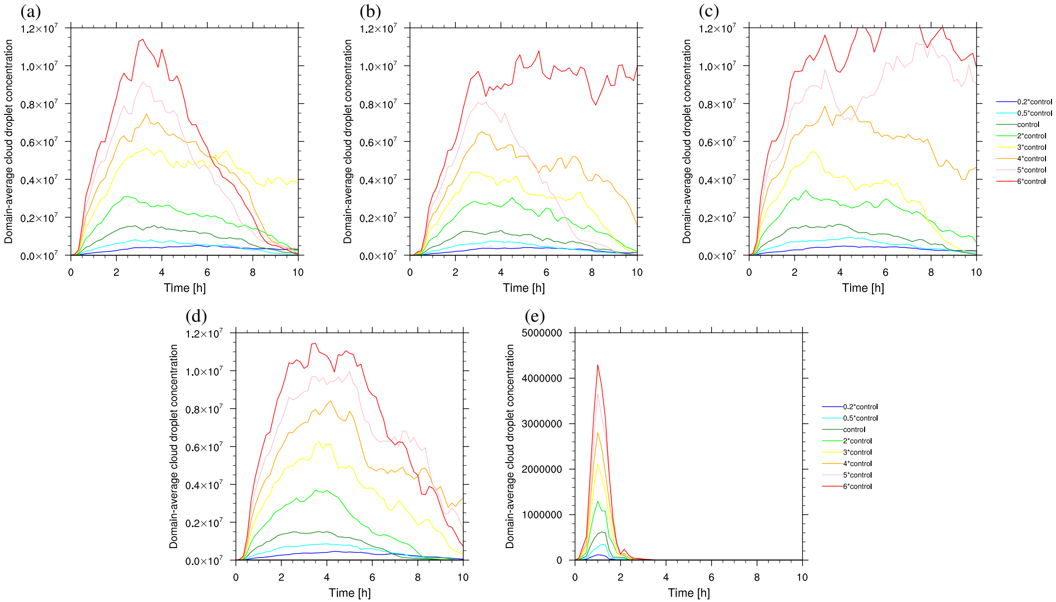

Figure 7. Time evolution of domain-averaged cloud droplet number concentration in the **(a)** standard, **(b)** 1 K-heating, **(c)** 3 K-heating, **(d)** 2 km-resolution, and **(e)** no initial wind runs. It is clear that some of the runs (the 4*control, 5*control, and 6*control runs in the standard simulations, the 5*control run in the 1 K-heating simulation, and the 6*control run in the 2 km-resolution simulation) have anomalously low domain-averaged cloud droplet number concentrations later in the simulations.

ACPD
14, 24087–24118, 2014

Sensitivity study of the aerosol effects on a supercell storm

A. Takeishi and T. Storelvmo

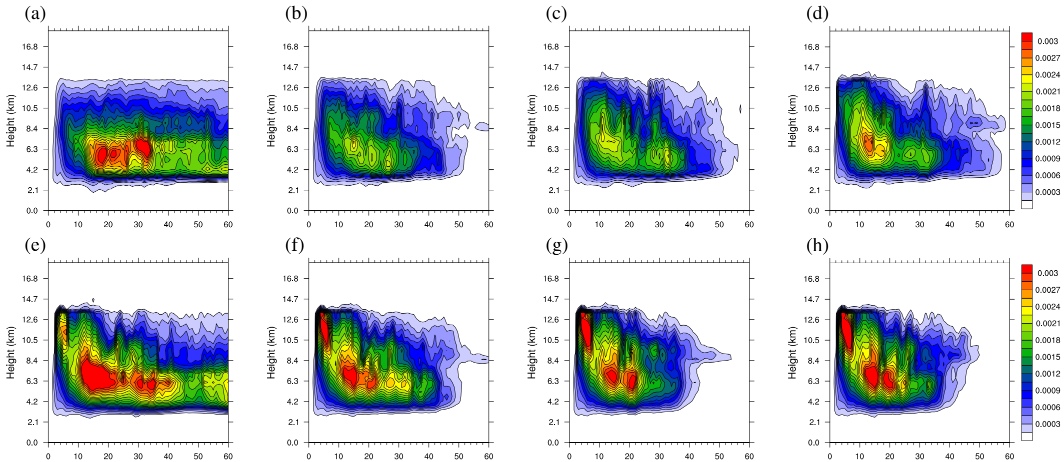

Figure 8. Time evolution of horizontally averaged liquid cloud mixing ratio [g kg^{-1}] in 8 runs with different aerosol concentrations; **(a)** 0.2*control, **(b)** 0.5*control, **(c)** control, **(d)** 2*control, **(e)** 3*control, **(f)** 4*control, **(g)** 5*control, and **(h)** 6*control in the Milbrandt–Yau runs. The vertical axis is height in [km], while the horizontal axis is time in [10 min], thus 60 corresponds to 600 min = 10 h.

ACPD
14, 24087–24118, 2014

Sensitivity study of the aerosol effects on a supercell storm

A. Takeishi and T. Storelvmo

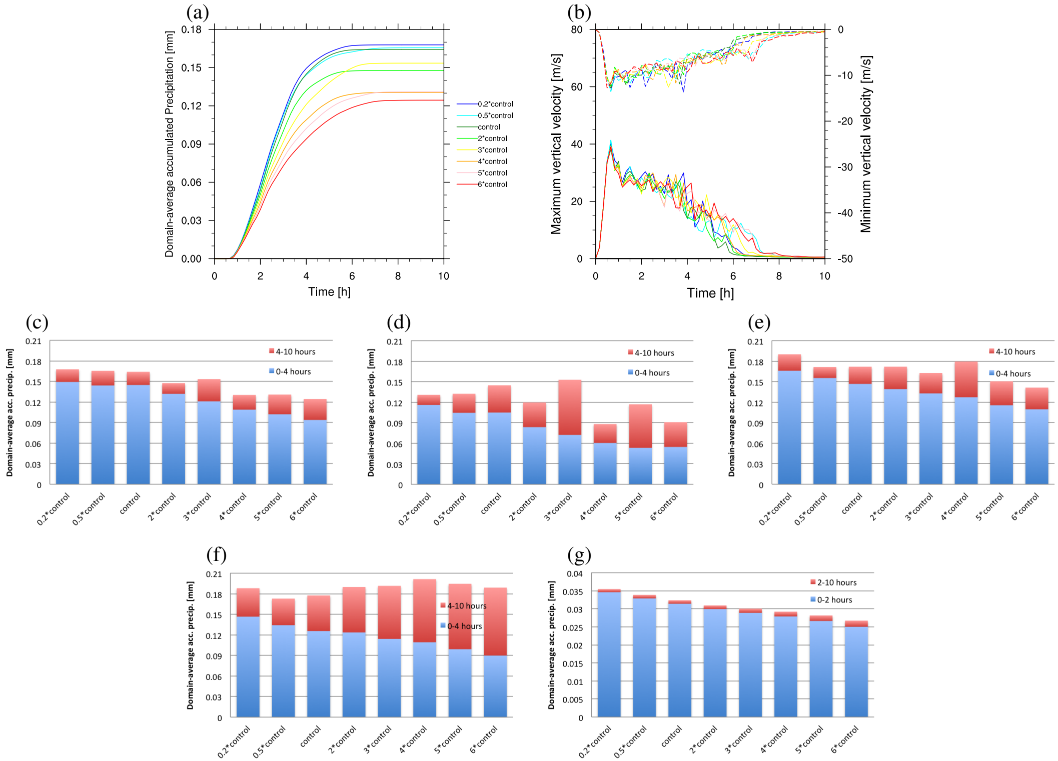

Figure 9. Results from simulations with the Thompson scheme; **(a)** time evolution of domain-average accumulated precipitation [mm] and **(b)** maximum (solid, left axis) and minimum (dashed, right axis) vertical velocities [$m\,s^{-1}$]. Different colors show runs with different aerosol concentrations. In addition, domain-averaged accumulated precipitation in [mm] with different aerosol concentrations in the **(c)** standard, **(d)** 1 K-heating, **(e)** 3 K-heating, **(f)** 2 km-resolution, and **(g)** no initial wind runs is shown.

ACPD
14, 24087–24118, 2014

Sensitivity study of the aerosol effects on a supercell storm

A. Takeishi and T. Storelvmo

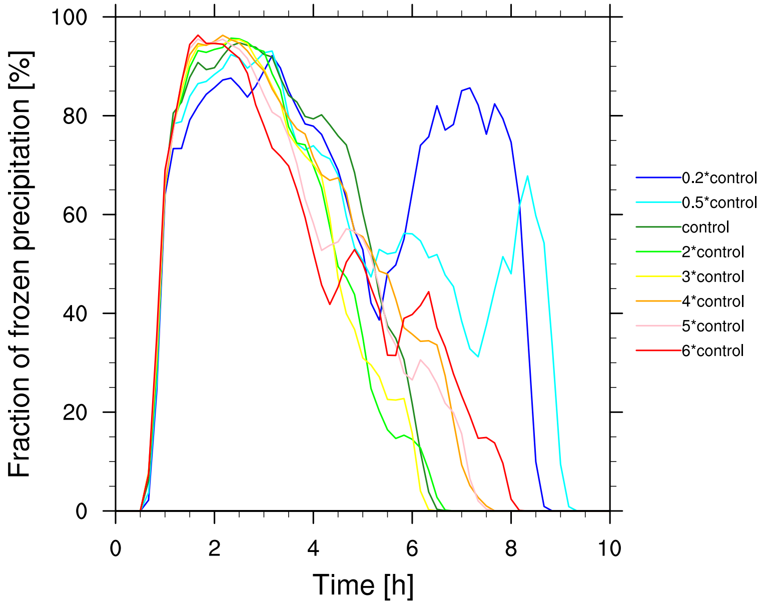

Figure 10. Time evolution of percentages [%] of frozen precipitation in total precipitation reaching the surface in past 10 min, when graupel does not melt in the runs with the Thompson scheme. If there is no surface precipitaiton in the past 10 min, the percentages are set to be zero.

ACPD
14, 24087–24118, 2014

Sensitivity study of the aerosol effects on a supercell storm

A. Takeishi and T. Storelvmo

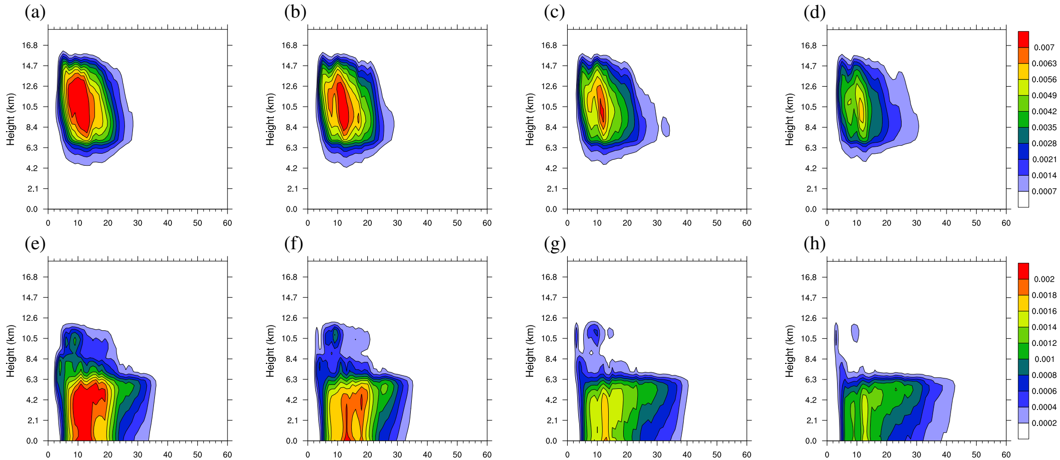

Figure 11. Time evolution of horizontally averaged graupel **(a–d)** and rain **(e–h)** mixing ratios [$\mathrm{g\,kg^{-1}}$] in **(a, e)** 0.2*control, **(b, f)** control, **(c, g)** 3*control, and **(d, h)** 6*control runs with the Thompson scheme. The vertical axis is height in [km], while the horizontal axis is time in [10 min], thus 60 corresponds to 600 min = 10 h.

ACPD
14, 24087–24118, 2014

A. Takeishi and T. Storelvmo

Title Page
Abstract | Introduction
Conclusions | References
Tables | Figures
◂◂ | ▸▸
◂ | ▸
Back | Close
Full Screen / Esc
Printer-friendly Version
Interactive Discussion

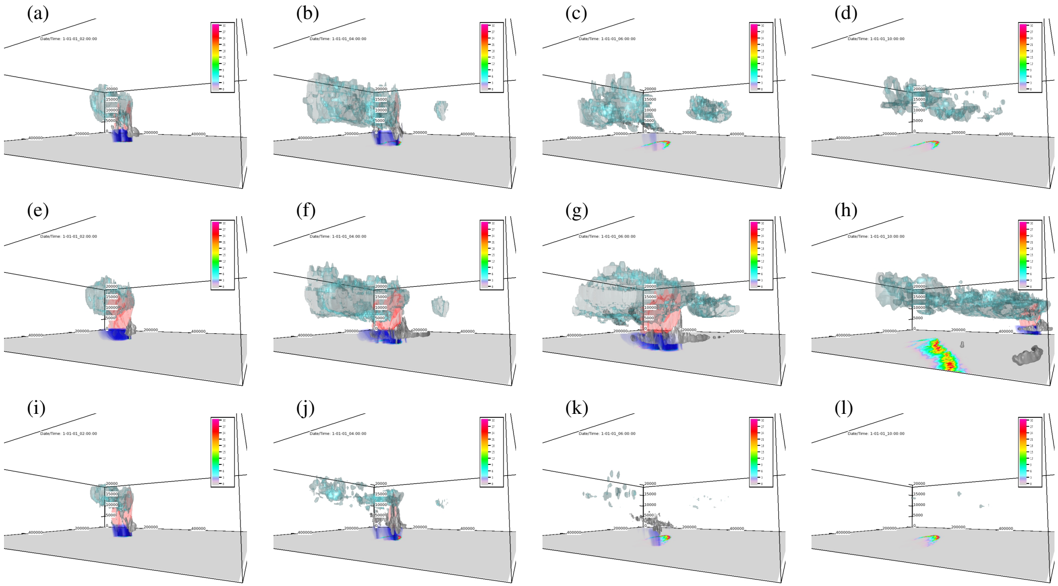

Figure 12. Isosurfaces of ice (cyan) mixing ratio of 0.001 g kg^{-1}, graupel (or hail in **a–d**, pink) mixing ratio of 1 g kg^{-1}, and liquid cloud (grey) mixing ratio of 0.1 g kg^{-1}, volume rendering of rain (blue), and the accumulated surface precipitation (surface colors, mm) in the cleanest case after 2 h **(a, e** and **i)**, 4 h **(b, f** and **j)**, 6 h **(c, g** and **k)**, and 10 h **(d, h** and **l)** of each simulation with the Morrison scheme **(a–d)**, the Milbrandt–Yau scheme **(e–h)**, and the Thompson scheme **(i–l)**.

ACPD
14, 24087–24118, 2014

Title Page
Abstract | Introduction
Conclusions | References
Tables | Figures
◀| |▶
◀ ▶
Back | Close
Full Screen / Esc
Printer-friendly Version
Interactive Discussion